Article

Effect of Nanoparticle Concentration on the Convective Deposition of Binary Suspensions

Pisist Kumnorkaew, and James F. Gilchrist

Langmuir, **Article ASAP** • Publication Date (Web): 27 April 2009

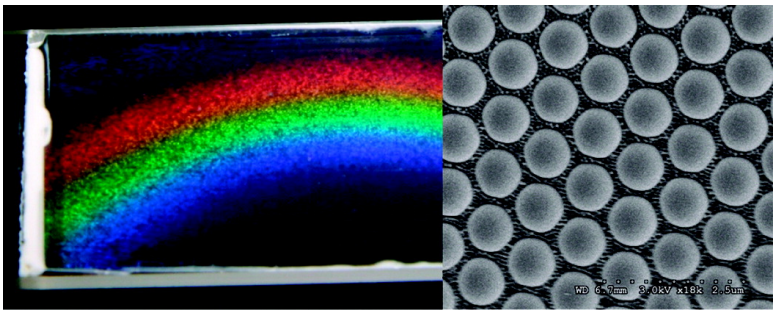

More About This Article

Additional resources and features associated with this article are available within the HTML version:

- Supporting Information
- Access to high resolution figures
- Links to articles and content related to this article
- Copyright permission to reproduce figures and/or text from this article

View the Full Text HTML

Langmuir
Article
pubs.acs.org/Langmuir

Effect of Nanoparticle Concentration on the Convective Deposition of Binary Suspensions

Pisist Kumnorkaew and James F. Gilchrist*

Center for Advanced Materials and Nanotechnology, Department of Chemical Engineering, Lehigh University, Bethlehem, Pennsylvania 18015

Received December 21, 2008. Revised Manuscript Received March 23, 2009

We investigate the coupling between the suspension properties and the deposition process during convective deposition of aqueous binary suspensions of 1 μm silica microspheres and 100 nm polystyrene (PS) nanoparticles. The structures formed from this rapid and scalable process have use in a variety of optical, chemical, and biochemical sensing applications. At conditions that produce a well-ordered microsphere monolayer at a silica volume fraction of 20% in the absence of nanoparticles, we examine the effect of varying the concentration of nanoparticles from 0% to 16% on the quality of the microsphere deposition and the exposure of the microspheres within the PS layer. At low concentrations of nanoparticles, the deposition results in an instability that forms stripes parallel to the receding contact line. Optimum deposition occurs between 6% and 8% PS and forms a monolayer having the same high degree of uniformity as the monodisperse suspension is fabricated. For higher concentrations, the deposition is increasingly less uniform as a result of nanoparticle depletion destabilizing the microspheres. The degree to which each microsphere is buried by the nanoparticles in the deposited thin film increases with nanoparticle concentration. This variation in coverage also suggests interplay between deposition and nanoparticle engineered properties of the suspension that influence the deposited morphology.

Introduction

There is great interest in developing methods to physically and chemically template surfaces. One such method, self-assembly of submicrometer size particles forming two-dimensional crystals on flat substrates, impacts fields including catalysis,[1] photonics,[2−4] lithography,[3,5,6]ceramics,[7] biocompatible surfaces,[8,9] and sensors.[9−11] Processes have been developed to facilitate particle deposition including spin coating,[12] epitaxy,[13,14] optical tweezers,[15] electrophoretic assembly,[16] and convective deposition.[17−19] Continuous convective assembly is a prime candidate for achieving a desired surface morphology due its scalability. By vertically withdrawing a hydrophilic substrate from a diluted particle suspension, colloidal particles crystallize on the substrate in the thin film following the receding meniscus, not unlike the "coffee ring effect".[20,21]

To broaden the classes of materials that can be fabricated via colloidal assembly, binary colloidal crystals of particles of comparable size or systems having a high particle size ratio where the small particles fill the interstitial sites have been investigated using a variety of techniques. This can be performed through layer-by-layer convective deposition.[22−24] Stepwise spin coating[25] and electric-field-induced assembly[26] are also used. These techniques require either two steps of fabrication or a complicated deposition process. Single step processes via accelerated convective deposition[27,28] have also been used. However, the use of diluted suspension in those studies results in a deposition time of several hours per centimeter of deposition, which is a significant limitation with regard to process scale up.

Recently, Velev and Prevo[29] developed a similar technique called rapid convective deposition using horizontal deposition of a microliter droplet where a concentrated suspension was injected between the deposition blade and substrate. The use of a small

*Corresponding author. E-mail: gilchrist@lehigh.edu.

(1) Tessier, P. M.; Velev, O. D.; Kalambur, A. T.; Rabolt, J. F.; Lenhoff, A. M.; Kaler, E. W. *J. Am. Chem. Soc.* **2000**, *122*, 9554–9555.
(2) Tessier, P. M.; Velev, O. D.; Kalambur, A. T.; Rabolt, J. F.; Lenhoff, A. M.; Kaler, E. W. *Adv. Mater.* **2001**, *13*, 396–400.
(3) Haes, A. J.; Haynes, C. L.; Richard, P.; Duyne, V. *Mater. Res. Soc. Symp. Proc.* **2001**, *636*, D4.8/1–D4.8/6.
(4) Im, S. H.; Lim, Y. T.; Suh, D. J.; Park, O. O. *Adv. Mater.* **2002**, *14*, 1367–1369.
(5) Haynes, C. L.; Van Duyne, R. P. *J. Phys. Chem. B* **2001**, *105*, 5599–5611.
(6) Zhang, Y.; Wang, X.; Wang, Y.; Liu, H.; Yang, J. *J. Alloys Compd.* **2008**, *452*, 473–477.
(7) Harris, D. J.; Hu, H.; Conrad, J. C.; Lewis, J. A. *Phys. Rev. Lett.* **2007**, *98*, 148301.
(8) Zhang, Y.; Wang, S.; Eghtedari, M.; Motamedi, M.; Kotov, N. A. *Adv. Funct. Mater.* **2005**, *15*, 725–731.
(9) Koyama, K.; Yamaguchi, N.; Miyasaka, T. *Science* **1994**, *265*, 762–765.
(10) Velev, O. D.; Kaler, E. W. *Langmuir* **1999**, *15*, 3693–3698.
(11) Yi, D.; Kim, M.; Turner, L.; Breuer, K.; Kim, D.-Y. *Biotechnol. Lett.* **2006**, *28*, 169–173.
(12) Jiang, P.; McFarland, M. J. *J. Am. Chem. Soc.* **2005**, *127*, 3710–3711.
(13) Blaaderen, A. V.; Hoogenboom, J. P.; Vossen, D. L. J.; Yethiraj, A.; Horst, A. V. D.; Visscher, K.; Dogterom, M. *Faraday Discuss.* **2003**, *123*, 107–119.
(14) Lee, W.; Chan, A.; Bevan, M. A.; Lewis, J. A.; Braun, P. V. *Langmuir* **2004**, *20*, 5262–5270.
(15) Biancaniello, P. L.; Crocker, J. C. *Rev. Sci. Instrum.* **2006**, *77*, 113702-10.
(16) Hayward, R. C.; Saville, D. A.; Aksay, I. A. *Nature (London)* **2000**, *404*, 56–59.
(17) Dimitrov, A. S.; Nagayama, K. *Langmuir* **1996**, *12*, 1303–1311.
(18) Shimmin, R. G.; DiMauro, A. J.; Braun, P. V. *Langmuir* **2006**, *22*, 6507–6513.
(19) Diao, J. J.; Hutchison, J. B.; Luo, G.; Reeves, M. E. *J. Chem. Phys.* **2005**, *122*, 184710-5.
(20) Deegan, R. D.; Bakajin, O.; Dupont, T. F.; Huber, G.; Nagel, S. R.; Witten, T. A. *Nature (London)* **1997**, *389*, 827–829.
(21) Deegan, R. D.; Bakajin, O.; Dupont, T. F.; Huber, G.; Nagel, S. R.; Witten, T. A. *Phys. Rev. E* **2000**, *62*, 756.
(22) Shyr, M. H. S.; Wernette, D. P.; Wiltzius, P.; Lu, Y.; Braun, P. V. *J. Am. Chem. Soc.* **2008**, *130*, 8234–8240.
(23) Kim, M. H.; Im, S. H.; Park, O. O. *Adv. Mater.* **2005**, *17*, 2501–2505.
(24) Velikov, K. P.; Christova, C. G.; Dullens, R. P. A.; van Blaaderen, A. *Science* **2002**, *296*, 106–109.
(25) Wang, D.; Möhwald, H. *Adv. Mater.* **2004**, *16*, 244–247.
(26) Huang, X.; Zhou, J.; Fu, M.; Li, B.; Wang, Y.; Zhao, Q.; Yang, Z.; Xie, Q.; Li, L. *Langmuir* **2007**, *23*, 8695–8698.
(27) Kitaev, V.; Ozin, G. A. *Adv. Mater.* **2003**, *15*, 75–78.
(28) Kim, M. H.; Choi, H. K.; Park, O. O.; Im, S. H. *Appl. Phys. Lett.* **2006**, *88*, 143127-3.
(29) Prevo, B. G.; Velev, O. D. *Langmuir* **2004**, *20*, 2099–2107.

amount of concentrated suspension in rapid convective deposition shortens the deposition time to minutes per centimeter of the deposition. In these experiments, the small droplet of suspension is held in place by the capillary forces between the blade and substrate, and translated using a linear motor. This technique allows the use of high particle volume fraction, $\phi_{bulk} > 10\%$, and faster monolayer deposition speed of 5−30 cm/h. They confirmed the relationship proposed by Dimitrov and Nakayama,[30] here simplified for monolayer conditions,

$$v_c = v_d = \frac{\beta J_e \phi}{0.605 d(1-\phi)} \quad (1)$$

The deposition rate v_d must be equal the crystal formation rate v_c which depends on particle volume fraction ϕ, evaporation flux of liquid J_e, particle size d, and a deposition parameter β. β has constant value between 0 and 1 depending on the particle−particle and particle−substrate interactions.[30] For low volume fraction and electrostatically stable particles, β approaches 1 and decreases as particle−substrate interactions increase.

As the substrate is pulled away from the bulk suspension, particles from the bulk suspension continue to move to the contact line in evaporation-driven liquid flow[20,31,32] in the thin film region and through convective flow from the moving substrate. The particles most often self-assemble into a hexagonal close-packed structure at the crystal front due to the large capillary force[33] generated when the particles are confined in the thin film near the air/liquid/substrate contact line. For a monolayer crystal growth, the contact line is assumed to be the crystal front; that is, the height of the meniscus at the crystal front must equal the particle diameter. If the meniscus height at the crystal front is less than the particle diameter, as in the case of higher rate deposition conditions, the incoming particles will not form a close-packed structure. On the contrary, for slower deposition speeds, if the height of the crystal front is greater than the particle diameter, a multilayer deposition occurs. A monolayer of particles with a random hexagonal close-packed structure was obtained only with the use of a single optimal deposition speed at a specified blade angle.[34] For deposition speeds above and below the optimal speed to form a monolayer, sub-monolayer and multilayer depositions are obtained, respectively. Other studies of deposition in the thin film created by an advancing meniscus have investigated the role of substrate conditions[35,36] and other deposition parameters including blade angle and blade hydrophobicity,[34] in which case the relationship in eq 1 does not necessarily hold.

Conventionally, the uniformity of 3D crystals is determined by the stability of the suspension. For instance, charge groups or polymers grafted on the particle surface are typically used to stabilize suspension particles. However, crystals fabricated under gravity or using electrostatic or steric stabilization do not form close-packed structures, resulting in cracking upon drying. An exception to this is when particles are stabilized via nanoparticle "haloing",[37] where nanoparticles involved in stabilization have no affinity for the larger species, thus allowing solid contact between particles in the sedimentation process. Similarly, a clear advantage of this rapid convective deposition is that the capillary forces create close-packed crystals. The role of particle stability in convective deposition has not been previously investigated. It has been assumed that strongly stabilized particles form more uniform crystals, avoiding interparticle and particle−substrate attractions prior to deposition.

This study is primarily concerned with making monolayers of larger silica microspheres that are partially submerged in a deposited array of smaller polystyrene (PS) nanoparticles. This morphology is useful for fabricating photonic coatings,[34,38] membranes,[39] and substrates having a highly organized periodic chemical pattern functionalized for bioMEMS sensors. The details regarding the deposition process have been previously described.[34] By performing convective deposition of binary suspensions, it is desirable to control the overall surface morphology and the degree to which the larger microspheres are buried within the final deposited layer. It is clear that the solution properties, specifically the ratio of nanoparticles to microspheres, influence both macroscopic and nanoscale properties of the deposited layer. Solutions of $\phi_{micro} = 0.2$ with varying volume fractions of nanoparticles, $0 \le \phi_{nano} \le 0.16$, are deposited at the optimum deposition speed obtained when $\phi_{nano} = 0$ to monitor the influence of nanoparticle concentration on the deposited surface morphology.

Materials and Methods

Suspension Preparation. The primary colloid suspension used in this work is prepared by dispersing silica microspheres (Fuso Chemical Co, Japan) having a density of 2.2 g/cm^3, average diameter of 1.01 ± 0.02 μm, and zeta potential of −48 ± 1 mV in deionized (DI) water with the volume fraction of 0.2. The suspension is dispersed using a sonic dismembrator (model 550, Fisher Scientific, Pittsburgh, PA) for 10 min and stirred for 30 min (Fisher Sci., model 550). A separate colloidal suspension of 100 nm polystyrene (PS) having a zeta potential of −59 ± 1 mV prepared at 0.35 in DI water (supplied by the Emulsion Polymer Institute at Lehigh University) is combined with the silica solution to achieve the desired volume fraction.

Substrate Preparation. Plain glass microslides (76 × 25 × 1 mm^3, Fisher PA) are used as the deposition blade, and glass coverslips (40 × 24 × 0.25 mm^3, Fisher PA) are used as the substrate for all samples. All glassware is cleaned by immersing in a piranha solution, 5:1 v/v sulfuric acid/hydrogen peroxide, for 30 min. The glassware is then rinsed with DI water until no residual acid remains, and the cleaned glassware is immersed in DI water before use. The back and bottom edges of the glass deposition blade are made to be hydrophobic by adding a thin coating of parafilm (Fisher PA). The contact angle on bare glass and on the hydrophobic surface is measured to be 10° and 105°, repectively, by imaging a 10 μL stationary droplet on the surface.

Deposition. The experimental setup was described previously.[34] This apparatus is contained within a humidity controlled environment, where all experiments were performed at 53% relative humidity and 24 °C. The deposition blade angle is fixed at 45° and positioned approximately 10 μm above the substrate, observed directly using a digital camera (Dinolite AM311S). The volume of the colloid suspension for each experiment is 10 μL.

Microstructure Analysis. Deposited monolayers are observed directly using scanning electron microscopy (SEM) and confocal laser scanning microscopy. A Hitachi 4300 field emission

(30) Dimitrov, A. S.; Nagayama, K. *Chem. Phys. Lett.* **1995**, *243*, 462–468.
(31) Wayner, P. C. *J. Colloid Interface Sci.* **1980**, *77*, 495–500.
(32) Stephan, K.; Zhong, L. C.; Stephan, P. *Heat Mass Transfer* **1995**, *30*, 467–472.
(33) Denkov, N.; Velev, O.; Kralchevski, P.; Ivanov, I.; Yoshimura, H.; Nagayama, K. *Langmuir* **1992**, *8*, 3183–3190.
(34) Kumnorkaew, P.; Ee, Y.-K.; Tansu, N.; Gilchrist, J. F. *Langmuir* **2008**, *24*, 12150–12157.
(35) Kraus, T.; Malaquin, L.; Schmid, H.; Riess, W.; Spencer, N. D.; Wolf, H. *Nat. Nano* **2007**, *2*, 570–576.
(36) Fan, F.; Stebe, K. J. *Langmuir* **2005**, *21*, 1149–1152.
(37) Tohver, V.; Smay, J. E.; Braem, A.; Braun, P. V.; Lewis, J. A. *Proc. Natl. Acad. Sci. U.S.A.* **2001**, *98*, 8950–8954.
(38) Ee, Y.-K.; Arif, R. A.; Tansu, N.; Kumnorkaew, P.; Gilchrist, J. F. *Appl. Phys. Lett.* **2007**, *91*, 221107.
(39) Velev, O. D.; Kaler, E. W. *Adv. Mater.* **2000**, *12*, 531–534.

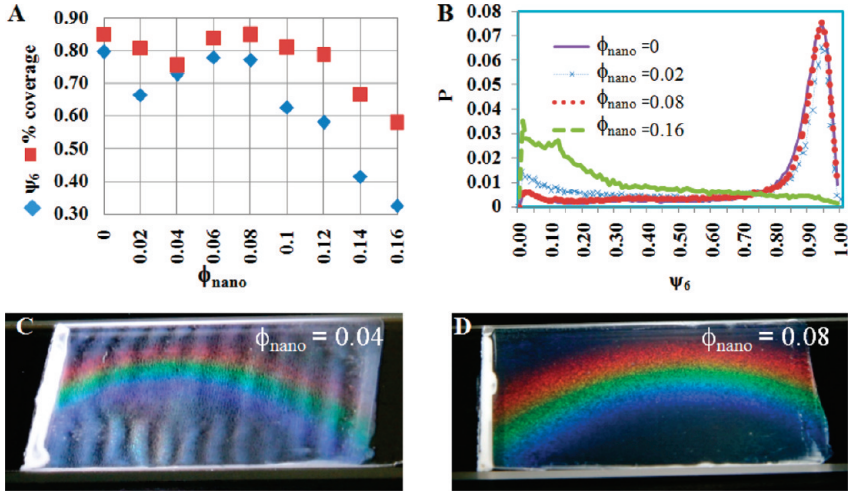

Figure 1. (A) Surface microstructure as evaluated by measuring substrate density, ρ, and surface crystallinity; $\psi_{6,ave}$ is a function of nanoparticle volume fraction. The optimum structure is recovered at $\phi_{nano} = 0.08$ and produces the largest coherent thin films per microliter of solution used in the deposition. (B) Probability distribution of ψ_6 plotted for $\phi_{nano} = 0$, 0.02, 0.08, and 0.16 shows similarities in microstructure for $\phi_{nano} = 0$ and $\phi_{nano} = 0.08$, and $\phi_{nano} = 0.16$ has few crystalline domains. (C,D) Images of samples show the variability of the deposition due to the addition of nanoparticles. At $\phi_{nano} = 0.04$ (C), we see variations in thickness from brighter stripes of crystalline monolayer to darker stripes of pure nanoparticles without microspheres. For $\phi_{nano} = 0.08$ (D), a continuous monolayer covers the entire substrate.

scanning electron microscope is used to observe the microstructure. Prior to SEM imaging, the sample is coated with iridium. Confocal laser scanning microscopy (VTeye, Visitech International) is used to observe the microstructure by rewetting the layer with an aqueous solution of 8 mM Rhodamine B for imaging which does not disturb the microstructure. The sample is scanned at 30 fps while translating the sample across the microscope objective at 100 μm/s using a motorized stage. This allows the scanning of large regions of the sample (~60 000 microspheres) to evaluate the microstructure of those microspheres in contact with the substrate; specifically, the relative microsphere substrate coverage, ρ, and the local bond order, ψ_6, were evaluated. The maximum theoretical value of surface coverage for monosized microspheres deposited as a single crystal is $\rho = \pi/(12)^{1/2} = 0.907$. The long-range nanoparticle substrate coverage is only qualitatively reported. Ψ_6 is a parameter that describes the relative orientation of particles around a central particle. It is calculated by using all angles θ between each particle of interest i and its nearest neighbors j. Prior to the computation, vectors r_{ij} are determined for all nearest neighbors N as shown by

$$\psi_6(r_{ij}) = \frac{1}{N}\sum_{j=1}^{N} \exp\left[6i\theta(r_{ij})\right] \qquad (2)$$

where $\psi_6 = 1$ is a perfect crystal and $\psi_6 \geq 0.8$ is highly ordered for a polycrystalline morphology.

Experimental Results

The most important result in this process is the observation that addition of nanoparticles to the microsphere suspension has a large effect on the morphology and the final uniformity of the microsphere monolayer. The long-range order, characterized by local bond order $\psi_{6,ave}$ and average microsphere substrate coverage density ρ_{ave}, is used to quantify the thin film quality and is shown in Figure 1. Without nanoparticles, the previously determined ideal deposition velocity for a suspension of monosized 1 μm microspheres is $v_d = 30$ μm/s for a deposition angle of $\alpha = 45°$. These conditions form a highly ordered monolayer having $\rho_{ave} = 0.85$ and $\psi_{6,ave} = 0.80$.[34] Nanoparticles are added to the solution, and the experiment is run using the same deposition conditions. Figure 1A shows a relative decrease in microsphere surface coverage and local order for $\phi_{nano} = 0.02$ and $\phi_{nano} = 0.04$ as compared to the monodisperse suspension, and a recovery in coverage near $0.06 \leq \phi_{nano} \leq 0.08$. For higher ϕ_{nano}, the surface coverage and crystallinity decrease sharply. The probability distributions of ψ_6 for $\phi_{nano} = 0$, 0.02, 0.08, and 0.16 are shown in Figure 1B, where it is clear that all samples besides $\phi_{nano} = 0.16$ have a significant fraction of crystalline regions. Samples at $\phi_{nano} = 0$ and 0.08 are essentially the same, and at $\phi_{nano} = 0.02$ a tail at lower ψ_6 exists. For $\phi_{nano} = 0.16$, little crystallization is seen.

When nanoparticles are added to solution at $\phi_{nano} = 0.02$, periodic spanwise bands of monolayers and bilayers oriented roughly parallel to the receding meniscus form spontaneously. The entire surface is covered with regions of mono- or bilayers with more total particles deposited than would be found in a single monolayer. Within each band, particles are oriented in randomly hexagonal close packed domains; however, the transition regions between monolayer and bilayer regions are more disordered and more regions of square packing are present, as reported previously.[29,40] This results in a decrease in $\psi_{6,ave}$, and because fewer microspheres are in contact with the substrate, a decrease in $\psi_{6,ave}$ as well. Vertical bands are also observed at the macroscopic scale for $\phi_{nano} = 0.04$, shown in Figure 1C; however, these bands differ from those observed at $\phi_{nano} = 0.02$ having alternating regions of monolayer and sub-monolayer morphologies. The sub-monolayer bands have local order with teardrop shaped patches of bare surface. The result is a decrease in ρ_{ave} due to a lower total surface coverage, and an increase in $\psi_{6,ave}$ because of the lack of transition regions between mono- and bilayers of particles. Bands resulting from convective deposition of monodisperse suspensions have been reported previously,[41,42] and successive meniscus pinning has been reported for drying suspension droplets.[43]

(40) Meng, L.; Wei, H.; Nagel, A.; Wiley, B. J.; Scriven, L. E.; Norris, D. J. *Nano Lett.* **2006**, *6*, 2249–2253.
(41) Ghosh, M.; Fan, F.; Stebe, K. J. *Langmuir* **2007**, *23*, 2180–2183.
(42) Lee, J. A.; Meng, L.; Norris, D. J.; Scriven, L. E.; Tsapatsis, M. *Langmuir* **2006**, *22*, 5217–5219.
(43) Maheshwari, S.; Zhang, L.; Zhu, Y.; Chang, H.-C. *Phys. Rev. Lett.* **2008**, *100*, 044503-4.

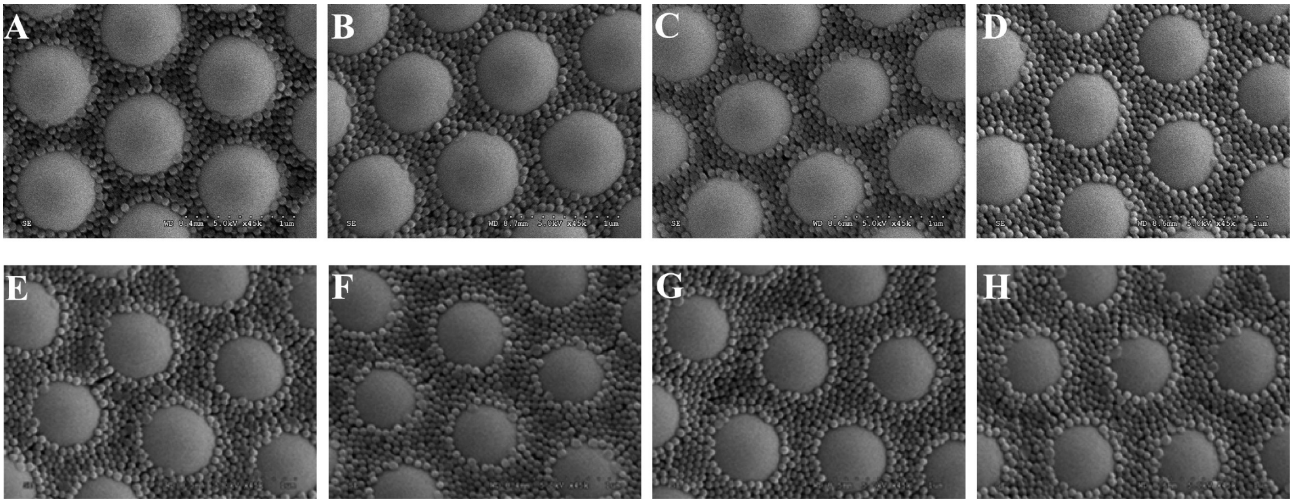

Figure 2. SEM images of the deposited morphology of microspheres partially buried by nanoparticles. All samples are created from solutions $\phi_{micro} = 0.2$ and $\phi_{nano} = 0.02$ (A), 0.04 (B), 0.06 (C), 0.08 (D), 0.10 (E), 0.12 (F), 0.14 (G), and 0.16 (H). Neighboring microspheres are in contact, and nanoparticles fill the interstitial regions up to a height less than the diameter of the microsphere.

Increasing the nanoparticle volume fraction to $0.06 \leq \phi_{nano} \leq 0.08$, well-ordered monolayers are deposited, as shown in Figure 1D. Very few small teardrop shaped patches exist at $\phi_{nano} = 0.06$; at $\phi_{nano} = 0.08$, the only imperfections are crystalline line and point defects. Increasing $\phi_{nano} > 0.08$, $\psi_{6,ave}$ and ρ_{ave} drop significantly, and sub-monolayers of disordered microspheres are formed at the highest nanoparticle volume fractions. These sub-monolayers have regions of higher microsphere density separated by regions covered only by nanoparticles.

The distribution of nanoparticles within the sample also varies greatly with increasing ϕ_{nano}. SEM images of deposited thin films having a monolayer of silica microspheres with PS nanoparticles filling the interstitial sites are shown in Figure 2. For samples $\phi_{nano} < 0.06$, only patchy regions have the morphology with interstitial regions completely filled with nanoparticles; other regions have microspheres with nanoparticles sparsely absorbed to their surface. In these experiments, selecting a large size ratio, here a 10:1 microsphere/nanoparticle ratio in diameter, is critical in having a relatively high degree of nanoparticle infilling.[23,27]

Two aspects of the deposition are readily apparent from these images. First, the amount of nanoparticle coverage of the microspheres is dependent on ϕ_{nano}. Analyzing these images, and confirming results with SEM images of fractured thin films that show nanoparticles completely filling the interstitial regions, we calculate the relationship between ϕ_{nano} and microsphere exposure (Figure 3). Over this series of experiments $0.02 \leq \phi_{nano} \leq 0.16$, this increase in microsphere coverage corresponds to a 42% decrease in exposed microsphere surface area. Second, it is clear from the SEM images in Figure 2 that the nanoparticles form highly dense structures and are not adsorbed to the top surface of the microsphere. Only localized nanoparticle ordering exists due to confinement in the interstitial spaces between microspheres. Some cracks in the nanoparticle assemblies are observed, which are presumably due to the final evaporative drying of the deposited layer far from the point of microsphere deposition.

After deposition and subsequent heating to bury the microspheres in a homogeneous polymer layer, samples were imaged using SEM (Figure 4) to evaluate the morphology. In crystalline regions of microspheres where the nanoparticles are well distributed, the PS wets the microspheres, leaving essentially the same microsphere exposure as that present prior to melting. The structure of the microspheres is essentially unaltered and the interstitial regions are filled with PS. This suggests that the PS interface between microspheres is concave; this is due to the densification of the PS phase from discrete close-packed particles to a dense continuous phase. This is confirmed in a side view image where PS wets both the substrate and microspheres (Figure 4C). In this image, a line defect separates two crystalline regions; in these regions, fewer particles are deposited and do not necessarily span the defect. Optimum coverage to maximize performance of nanoparticle/microsphere monolayers when used for LED applications is half-coverage of the microspheres,[44] and defects not filled with PS would adversely affect performance. For this reason, efforts to form larger regions of highly ordered microspheres is ongoing.

Discussion

It is unclear exactly how nanoparticle concentration dictates the microsphere exposure and the local microsphere crystallinity. There are four ways in which nanoparticles directly alter the deposition as related to quantities contained in eq 1. First, the deposited nanoparticles change the evaporative flux by exposing less surface area and by changing the Laplace pressure, due to changes in the local surface curvature related to the particle size and the difference in contact angle of water on PS versus that on silica. Although the surface area associated with flux is reduced by the presence of nanoparticles, the liquid layer may adjust to cover larger overall area to maintain a constant flux.[29] The wetting properties were not studied here, but by assuming that the contact angle is similar, the local radius of curvature on the surface will scale with the particle size. This effect could enhance evaporation with the introduction of nanoparticles. The result is to increase v_c due to the increased pressure drop across the thin film, or for a constant deposition speed resulting in multilayer deposition. Second, the deposited nanoparticles decrease the void fraction significantly for fluid transport to the evaporative region within the deposited layer. Decreasing the void fraction will reduce the flow rate within the thin film for a constant pressure drop between the evaporation region and the bulk suspension. Third, the addition of nanoparticles alters the effective viscosity of the solution, which in turn alters the flow rate for a given pressure

(44) Ee, Y.-K.; Kumnorkaew, P.; Tong, H.; Arif, R. A.; Gilchrist, J. F.; Tansu, N. *Light-Emitting Diodes: Research, Manufacturing, and Applications XII*, 1st ed.; SPIE: San Jose, CA, 2008; Vol. 6910, p 69100M-8.

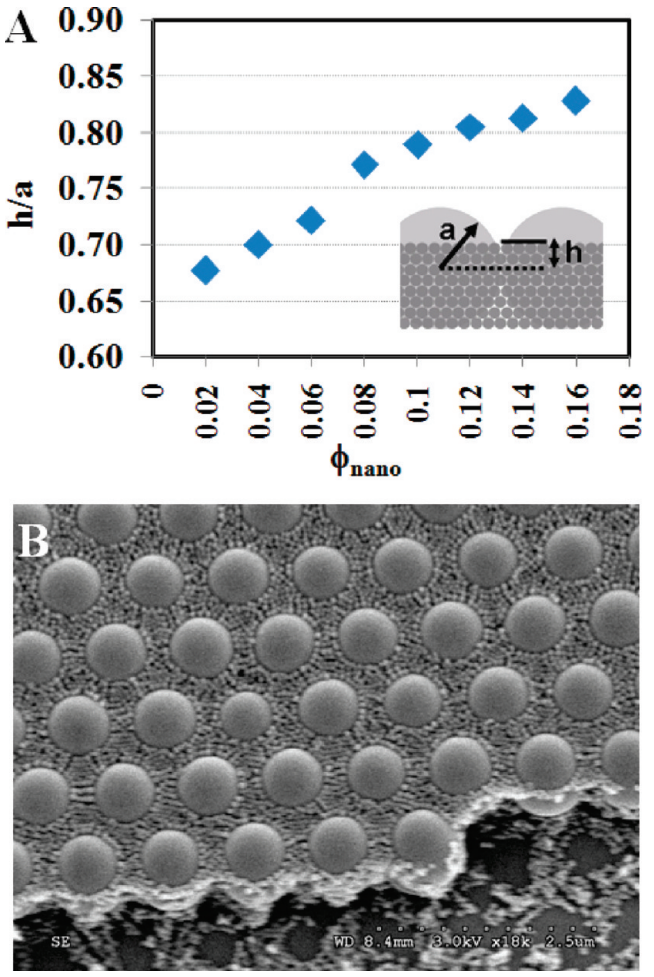

Figure 3. (A) Relative burial of microspheres by nanoparticles as determined from image analysis of Figure 2 and from images of cracked samples as shown below (B) that confirm complete interstitial filling by the nanoparticles. The height, h, above the midline of the microsphere of radius $a = 0.5\ \mu$m is a function of nanoparticle concentration.

drop. In this study, the volume fraction of microspheres is low enough that the addition of nanoparticles should increase the viscosity, which should decrease v_c. Fourth, the addition of nanoparticles changes the stability of the microspheres in solution. This effect is highly nontrivial at these concentrations. Direct observation of the deposition for $\phi_{nano} = 0.08$ shows microsphere clustering in the thin film region. It is well-known that the introduction of a smaller species can stabilize or destabilize suspensions of larger spheres.[45] In sediments deposited from static samples, the sediment is crystalline until $\phi_{nano} > 0.08$, suggesting the higher nanoparticle concentrations tested destabilize the microspheres through depletion aggregation.

Considering the above arguments, at $\phi_{nano} = 0.02$, the multilayer deposition may be the result of an increase in the evaporative flux, which increases the withdrawal rate of fluid through the pores. This alters the viscosity only slightly and has little effect on the particle stability. A decrease in surface density at $\phi_{nano} = 0.04$ results in lower $\psi_{6,ave}$ and may be the result of a decrease in the evaporative flux coming from the increase in suspension viscosity, which effectively decreases v_c. For $\phi_{nano} \geq 0.08$, nanoparticle depletion destabilization of the microspheres most likely causes the sub-monolayer microsphere deposition and lack of

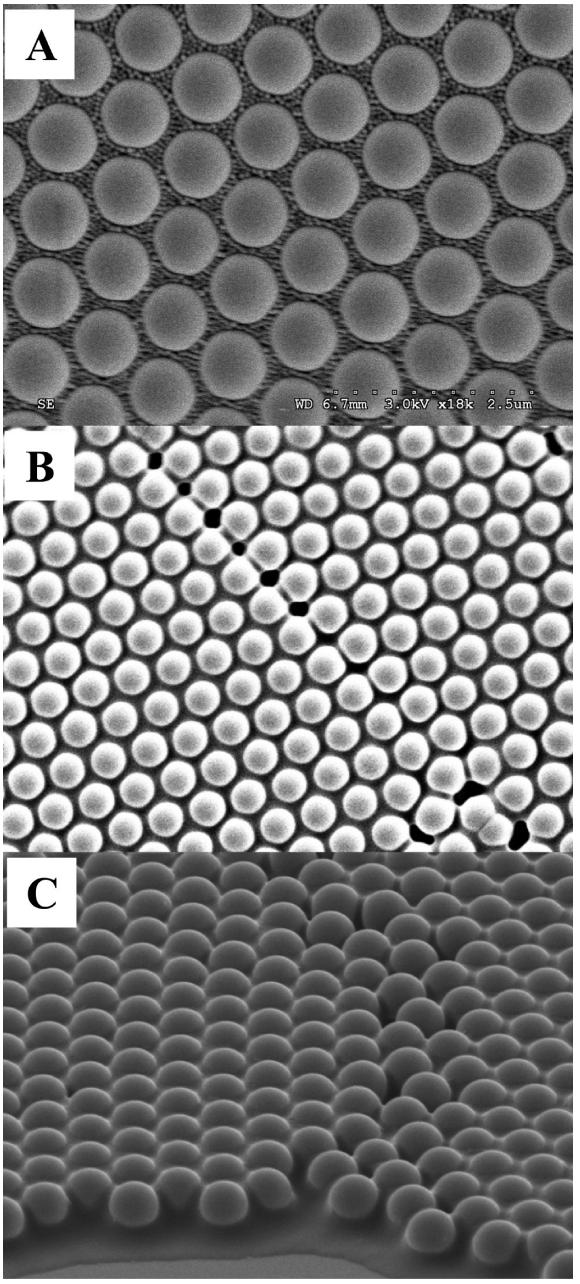

Figure 4. Highly uniform deposited monolayers of microspheres having interstitial regions filled with nanoparticles (A) retain their crystallinity after applied heat above 240 °C (B). At lower nanoparticle coverage, the wetted PS is absent from regions having defects, as seen in the middle image highlighting a line defect where the black region shows local dewetting of the PS layer. The side view image (C) shows the edge of a monolayer demonstrating that the PS is wetted throughout the interstitial regions between microspheres in regions of high order.

crystallinity. This description is insufficient for understanding why well-ordered monolayers are formed for $0.06 \leq \phi_{nano} \leq 0.08$. Simply considering microsphere stability, it is possible that microsphere−microsphere interactions result in enhanced crystallinity through depletion stabilization.[46] The microspheres are electrostatically stable at $\phi_{nano} = 0.04$, depletion stabilized near $\phi_{nano} = 0.08$, and depletion destabilized at higher nanoparticle concentration. Further variations on this experiment may allow a

(45) Asakura, S.; Oosawa, F. *J. Polym. Sci.* **1958**, *33*, 183–192.

(46) Trokhymchuk, A.; Henderson, D.; Nikolov, A.; Wasan, D. T. *Phys. Rev. E* **2001**, *64*, 012401.

 DOI: 10.1021/la804209m

direct and dynamic method of probing of the stability of the microspheres.

These arguments however do not explain the stripes formed at lower nanoparticle concentrations. An alternative theory explaining this phenomenon stems from consideration of the fluxes of the individual species. Since depositions of $0.06 \leq \phi_{nano} \leq 0.08$ result in relatively homogeneous monolayers, it is reasonable to assume that the flux of microspheres and the flux of the nanoparticles are equal. Thus, for lower ϕ_{nano}, the rate at which nanoparticles fill the interstitial spaces between microspheres is low, which creates a periodic instability when the nanoparticle deposition front is sufficiently far from the microsphere deposition front. An effective depinning of the meniscus occurs, and the process resets. This explanation is analogous to that proposed in previous studies describing stripe formation.[41,42] At higher ϕ_{nano}, perhaps in the absence of depletion destabilization, the deposition would be driven primarily by the nanoparticle flux, and microspheres might be carried into the thin film region at a lower deposition rate and would create a similar instability that might form stripes. An investigation of this hypothesis is ongoing.

Conclusion

Added nanoparticles alter the convective deposition of larger microspheres. Well-ordered microsphere monolayers form at $0.06 \leq \phi_{nano} \leq 0.08$ with nanoparticles filling the interstitial regions between the microspheres. Lower ϕ_{nano} demonstrates an instability that causes stripes of varying morphology, and higher ϕ_{nano} leads to the formation of dense regions of disordered microspheres due to depletion interactions. The height of the deposited nanoparticles in regions for which they surround the microspheres also is a function of ϕ_{nano}, where higher ϕ_{nano} results in higher microsphere coverage. The final microsphere structure is retained upon melting of the PS; however, the PS does not wet defects in the planar microsphere crystal. Further investigations to understand the interplay between the deposition parameters and the added nanoparticles are ongoing, and upon elucidating these details the deposition process itself could be used as a method of studying the effect of nanoparticles on microsphere stability.

Acknowledgment. We acknowledge laboratory assistance by Thanh Ta and Andrew Tadros and discussions with Alex Weldon. This work is based upon work supported by the National Science Foundation under Award Number 0828426. P.K. appreciates support by the Royal Thai Scholarship.

Supporting Information Available: Movies of lateral scans of select samples to highlight the surface morphology, and static images of sediment formed from the individual binary suspensions are shown to demonstrate the microsphere stability in each solution. This material is available free of charge via the Internet at http://pubs.acs.org.